Paper No.
09213

NACE INTERNATIONAL CORROSION 2009 CONFERENCE & EXPO

SERVICE LIFE FORECASTING FOR REINFORCED CONCRETE INCORPORATING POTENTIAL-DEPENDENT CHLORIDE THRESHOLD

A. A. Sagüés, S.C. Kranc, and K. Lau
Dept. of Civil and Environmental Engineering, University of South Florida
4202 E. Fowler Ave. ENB118
Tampa, FL 33620

ABSTRACT

The chloride corrosion threshold of steel in concrete depends not only on concrete and steel properties but also on the potential of the steel while it is still in the passive condition. A deterministic model to predict corrosion in reinforced concrete structures is presented, incorporating potential dependence and corrosion macrocell effects, resulting in coupling of the corrosion initiation and propagation stages. The model is applied to a generic partially submerged reinforced concrete marine pile. An analysis is made of sensitivity of model output to input parameters including the rate of dependence of threshold on potential, concrete resistivity, oxygen diffusivity and size of the steel zone activated upon reaching the chloride threshold. The results are contrasted with those of a comparable system where the threshold is not potential dependent.

Keywords: modeling, chloride threshold, potential, corrosion, steel, concrete

INTRODUCTION

Service life forecasting models for concrete structures exposed to environments corrosive to the reinforcing steel customarily address two stages of deterioration[1]. The first or initiation stage concerns the period from the moment the structure in placed in service until breakdown of steel passivity occurs. That event, in chloride rich environments, corresponds to the chloride content of the concrete at the steel surface having reached a critical threshold value C_T. The second or propagation stage is the subsequent period of active steel corrosion and accumulation of corrosion products, ending with concrete cracking or spalling with consequent need for repair or replacement. Service life (or duration until repair need) is then obtained as the sum of the duration of both stages.

For projecting the duration of the initiation stage, models assume a mechanism for chloride accumulation at the rebar surface. The mechanism is commonly based on diffusional transport and the system geometry, and may include various concrete properties in more

sophisticated treatments[2,3] . Values of the transport parameters chosen to represent the system conditions are then used to calculate the amount of time needed for concentration at the steel surface to reach a similarly chosen value of C_T. The duration of the propagation stage is sometimes taken to be a single value representative of the system[4], or calculated based on expected corrosion rate (or calculated rate if kinetic parameters governing the corrosion process are known[5]) and the amount of corrosion needed to crack the concrete cover[6].

In extended systems the length of the initiation and propagation stages may change from point to point due to spatial variability of the model parameters, and treatments including appropriate statistical distributions of those parameters have been presented[7-11]. Spatial variability in C_T due to different local conditions or to inherent dispersion of that parameter[12-14] has been introduced as well, leading to a more realistic representation of the development of corrosion in actual structures. However, those treatments tend to neglect coupling between the initiation and propagation stages of nearby regions, especially pertaining the effect of that coupling on the value of C_T.

There is increasing recognition[15-17] that C_T depends on the value of the potential E of the passive steel with respect to the surrounding concrete. The dependence is such that C_T tends to increase as E becomes more cathodic [(1)]. As it is well known, the first corrosion initiation event in a previously passive reinforcing steel assembly shifts the local potential toward more negative values. Galvanic coupling with the surrounding, still passive steel makes its potential more negative than before the onset of active corrosion nearby. The value of C_T in that surrounding steel becomes therefore greater than it was for the spot first activated. Similar events occur as other portions of the assembly become active as a result of increasing chloride intrusion with time. Thus, the local value of C_T in the remaining portions of the structure where steel is still passive can be significantly greater than that encountered at the first spot that underwent activation. Corrosion in those remaining places is therefore prevented until the chloride content reaches a substantially increased local value of C_T, correspondingly increasing the length of the initiation stage there and resulting in a slower progression of damage with time that if C_T had a time-invariant value. This phenomenon has consequences widely recognized in other areas (e.g. cathodic prevention[16-17] and the "halo" effect on concrete patch repairs[18], but it has received relatively little attention in current predictive models for corrosion damage in reinforced concrete. That situation stems in part from complexities in quantitative modeling implementation but, more notably, from scarcity of data on the C_T-E relationship. Recently improved knowledge on the latter[1-2] put implementation of a potential-dependent threshold feature within reach of practical predictive models.

The purpose of this paper is to establish and illustrate the concept of a functional approach to implement potential dependent threshold in corrosion damage projections, plus integration of the initiation and propagation stages, in one predictive model. Preliminary work toward that end was previously introduced by the authors [19,20]. That approach is revisited here with emphasis in establishing sensitivity to the choice of model parameters and other issues relevant to incorporation in practical forecasting models. This investigation expands the

---

(1) This dependence parallels the well-recognized relationship between pitting potential and chloride concentration in localized corrosion[21] but it may also reflect to some extent beneficial compositional changes (such as decrease in chloride content and pH elevation) at the steel-concrete interface[16].

number and range of variables investigated in previous work[20]. Remaining issues are being addressed in continuation studies.

MODELING

Approach

The model is illustrated with an idealized representation of a partially submerged marine substructure column of reinforced concrete that can be implemented in two or three dimensions[19,22] or, as used here, as a simplified one-dimensional simulation sufficient to address the questions at hand. Chloride ions penetrate through the concrete cover toward the embedded steel bar (rebar) assembly, which is divided into elements each corresponding to a node in a linear array spanning the elevation range from the submerged to the above-water portions of the column. The external concrete surface was assigned a time-invariant chloride concentration profile, highest near the waterline where splash-evaporation is prevalent[23].

The rebar assembly was assumed to be initially passive, undergoing anodic dissolution at a small current density. Once an element of the assembly became active (starting near the waterline where chloride ingress was fastest), anodic dissolution was assumed to proceed at that element under active condition at a faster rate determined by assumed kinetic parameter values. The cathodic reaction, oxygen reduction, was assumed to proceed under combined activation-concentration polarization at rates also determined by assumed kinetic parameters, and an assumed oxygen diffusivity profile.

The model program consisted of modules calculating the system condition at each consecutive time step. For each step, a *corrosion distribution module* computed the potential and corrosion rate of the steel at each element based on the passive/active character of the steel there as determined in the previous time step, and solving the system of polarization equations and electrolyte conduction equations for the array. The resulting steel potential at each point was used to calculate the corresponding new value of C_T at each node, based on a potential-C_T function and parameters that were part of the model inputs. A *chloride transport module* calculated next for each steel surface node the chloride concentration, and compared it with the newly calculated value of C_T. If the concentration was found to exceed C_T, the steel element for that node was declared to be active for the purposes of the corrosion distribution module in the next time step. The local corrosion rate at the element for each node was integrated as a function of time and converted into local corrosion penetration by means of the *surface damage evaluation module*. This module also compared the local penetration with a value P_{crit} assumed to result in concrete cover cracking/spalling for the combination of rebar diameter and concrete cover used at that location of the system[6,24]. When P_{crit} was reached at a given steel element, the steel element area projected on the external concrete surface was counted as a damaged concrete area. The sum of damaged concrete area for the entire system as a function of time, expressed as a fraction of the total external concrete area, was defined as the *damage function* of the system.

It is noted also that this approach powerfully integrates the initiation and the propagation stages of corrosion in a single predictive model. The model includes not only the effect of the regions already undergoing corrosion in delaying corrosion initiation elsewhere, but also the effect of macrocell development in accelerating/slowing corrosion propagation after activation of different zones of the steel assembly. The potential of the above approach was

demonstrated in preliminary work[19] by illustrations of evaluation of the effectiveness of corrosion mitigation procedures for the propagation stage of corrosion, including the use of submerged and surface galvanic anodes, and corrosion inhibitors.

System Details

The system is a marine substructure, solid cylindrical reinforced concrete column partly submerged in seawater. An idealized, one-dimensional model was employed to represent the column, essentially identical to that used by the authors related work reported elsewhere[25]. As shown in that work, this simplified approach captures most of the features of interest of the system with minimum computational effort. Except for description of the variations on concrete resistivity and oxygen diffusivity, much of the methodology description presented in the following five subsections is identical to that discussed in Ref. 20, and it has been reproduced here in the following indented text for clarity and completeness.

> The column has a total height L, diameter Φ, and a single rebar mat placed at a cover depth X_C from the surface. The rebar mat, treated as a uniform sheet, has a total surface area of steel exposed to concrete equal to the external lateral column surface area multiplied by a Steel Factor S_F. The ends of the cylindrical column are considered to be isolated electrically and from the surrounding environment, and with no reinforcement. The column is assumed to be immersed in seawater to half its length. The concrete is approximated as an effectively homogeneous electrolytic medium of resistivity ρ, and effective oxygen diffusivity D_O both functions of elevation, and an effective chloride ion diffusivity D treated here for simplicity as a constant but the choice is not limiting. Concrete on the lateral surface of the column is assumed to have developed very early a time-invariant chloride ion concentration C_S that is a function of elevation, and a time-invariant effective oxygen concentration C_{SO} . C_{SO} is on first approximation treated as being constant with elevation as reflecting equilibrium between atmospheric oxygen and the pore water at the surface of the concrete (as wall as with seawater). However, the effect of salinity variations on C_{SO} is ignored for simplicity.
>
> The reinforcing steel is assumed to be the locus of an anodic metal loss reaction,
>
> $$Fe \rightarrow Fe^{2+} + 2e^{-} \qquad (1)$$
>
> with a corresponding current density i_a, under two modalities: passive dissolution at a fixed small current density i_p, or active dissolution at a potential-dependent current density i_{aa} so that
>
> $$i_a = i_p \qquad \text{(passive case)} \qquad (2a)$$
>
> $$i_a = i_{aa} = i_{oa}\, 10^{(E-Eoa)/\beta a} \qquad \text{(active case)} \qquad (2b)$$
>
> where i_{oa} is the nominal exchange current density, E is the steel potential with respect to an ideal reference electrode placed in the concrete immediately next to the steel, Eoa is the nominal equilibrium potential and β_a is the anodic Tafel slope. The steel is also assumed to support a single cathodic reaction, oxygen reduction:
>
> $$O_2 + 2H_2O + 4e^{-} \rightarrow 4OH^{-} \qquad (3)$$

which is considered for simplicity to occur under either a fully activation-controlled or a fully diffusion-limited conditions. Under full activation control the current density is

$$i_c = i_{ca} = i_{oc}\ 10^{(Eoc-E)/\beta c} \quad (4)$$

where i_{oc} is the nominal exchange current density, Eoc is the nominal equilibrium potential and β_c is the cathodic Tafel slope. Under full diffusional control the current density is

$$i_c = i_{cd} = 4\ F\ C_{SO}\ D_O / X_C \quad (5)$$

where 4 is the number of electrons to reduce O_2, F = 96.5 10^3 coul/equiv is Faraday's constant, C_{SO} is the oxygen concentration in the pore water at the external concrete surface, and D_O is the effective diffusion coefficient of O_2 in the concrete, scaled to match the concentration units used. The value of i_c is made to switch from i_{ca} to i_{cd} when the former exceeds the latter, creating a working approximation in lieu of the more computationally intensive mixed polarization function[26].

For both anodic and cathodic reactions the corresponding reverse reactions are ignored as the potentials of interest are assumed to be far away from the respective actual equilibrium potentials.

Chloride transport module

The chloride concentration C at the rebar depth X_C is calculated for regularly spaced times counting from the moment the structure is put in service. It is assumed for simplicity that diffusion behavior is ideal, initial bulk contamination is zero, and that $Xc << \Phi$ (nearly flat wall condition) so at a moment t

$$C(t) = C_S\ (1-\mathrm{erf}(Xc / (4Dt)^{1/2}) \quad (6)$$

Possible macroscopic effects of electric fields inside the concrete due to macrocell formation on chloride transport are ignored for simplicity.

Corrosion distribution module

Calling x the distance along the column axis, defining and treating the problem as one-dimensional in a manner similar to that used in Ref.25 the charge conservation condition implies that

$$i_S = (\Phi/4\ S_F)\ (\ \rho^{-1}\ d^2E/dx^2 + d(\rho^{-1})/dx\ \ dE/dx) \quad (7)$$

where $i_S = i_a - i_c$ is the net current density on the steel surface at elevation x , with i_a being equal to i_{aa} or i_p depending on whether the local steel surface was declared active or passive respectively if the value of C was respectively above or below the value of C_T.

Solution of Eq. (7) to obtain i_S and E as function of x is conducted iteratively for each time t using finite differences on a 101-node equispaced array along the elevation direction. As a check of solution convergence the percent difference between total

anodic and cathodic currents in the column was calculated, and verified to be normally substantially less than 1%.

The choice of the potential-C_T function was made based on recent work[16] indicating that in the potential range of interest

$$C_T \sim C_{Ts} 10^{(E_P - E)/\beta_{CT}} \quad (8)$$

where E is the passive steel potential, C_{Ts} is the threshold value at a baseline potential E_P (i.e. in atmospherically exposed concrete, for passive steel that has not yet undergone any galvanic coupling to active steel), and β_{CT} is the characteristic inverse slope of the increase of C_T in an E-logC_T representation.

The declaration of whether the steel element for a given node is in the active or passive condition is made using the value of C(t) from Eq. (6), and the local value of C_T calculated at each node per Eq.(8) using the value of E obtained at the end of the iterative solution process conducted in the previous time step. The array of values of C_T remains unchanged during the iteration process. After iteration is complete the potential array is used as seed for the next time step potential calculations. It is noted that once the steel element for a given node is declared active, it is declared to remain so for all subsequent time steps. This is only a simplifying assumption that may be refined in future implementations of the modeling concept.

Surface damage evaluation module

The value of i_a is integrated over time for each steel element, to obtain a cumulative anodic charge density (q_a) array. The anodic charge density at each element is Faradaically converted into a corrosion penetration depth P_C

$$P_C = A_{WFe}\, q_a / 2\, F\, \rho_{Fe} \quad (9)$$

where A_{WFe} = 55.85 g/mol is the atomic weight of Fe and ρ_{Fe} = 7.8 g/cm^3 is the density of Fe.

For each time t and at each steel element the value of P_C is compared with the critical penetration depth P_{CRIT} that results in appearance of a crack/spall [(2)] at the surface of the concrete[8] for the conditions encountered. If $P_C > P_{CRIT}$ the concrete over the steel element is declared damaged. For the present simplified model, possible effects of the appearance of cracks on subsequent corrosion development in the column are not addressed. Importantly, the present model (as well as an earlier rotational-symmetry 2-dimensional approach[19]) is limited to treat all points at a given elevation equally so lateral corrosion macrocells are not addressed either.

[(2)] The crack is assumed to be associated with simultaneous delamination of size comparable to the steel element area projected on the external concrete surface. The term "spall" is used here broadly to designate a delamination or the loss of concrete that would result if the delaminated portion were to fall off.

Summary of model inputs and outputs

Per the discussion above, the model inputs consist of the column dimensions; rebar mat depth and steel factor; concrete resistivity, oxygen diffusivity and chloride diffusivity elevation profiles; steel electrochemical kinetic parameters; surface chloride and oxygen concentration profiles; and value of critical corrosion penetration. Basic model outputs as function of time are the chloride content at the rebar depth and the steel potential elevation profile. From those are derived the reaction current density profiles; corresponding declarations of active/passive steel condition profiles, and cumulative damage profile as well as integrated column damage. In the terminology of Tuutti's initial corrosion damage concepts[1], the corrosion initiation stage at each node ends with the declaration of active condition, and the propagation stage starts with the activation declaration and ends with the damage declaration when P_{CRIT} is exceeded. The duration of both stages varies from steel element to element.

Base case and variations.

Again, following Ref 20, the input parameter values for a base case and variations of conditions are listed in Table 1, and these parameter distributions are also shown as functions of elevation in Figure 1. The dimensions selected for the column, concrete cover and steel placement density represent typical values encountered in marine substructures. As noted earlier, chloride diffusivity was assumed (for simplicity) to be an elevation-independent representative value. Modeling functions for concrete resistivity and oxygen diffusivity with elevation were more realistic, e.g. for the waterline/high tide level the resistivity was assigned a low limit value and above that level the resistivity was assumed to increase linearly with elevation. The limit values of those regimes were chosen to approximate actual observations in the field for low permeability concrete (with some adjustment for the one-dimensional approach, see note in Table 1) [27]. Manifestations of corrosion threshold dependence on potential result from corrosion macrocell coupling between active and passive zones, which in turn tends to be stronger as the concrete resistivity decreases. To explore the effect of this parameter in the model output the shape of the resistivity-elevation profile was kept the same, but variations involved values that at each elevation were 3 and 10 times smaller than in the Base case, thus spanning a range of resistivity comparable to that encountered in the field[11] . In addition to changing resistivity only, an additional series of cases was calculated using linked resistivity - chloride diffusivity variations. It is well known that for similar humidity conditions, concrete resistivity and chloride diffusivity tend to be roughly inversely correlated[28-30]. For those additional linked variations the value of D_{Cl^-} was still kept for simplicity space-invariant, but assigned a value $D_{Cl^-} = D_{Cl^- Base} \times \rho_{LBase} / \rho_{LVariation}$, where the subscripts Base or Variations indicates the value of ρ_L in the Base case or in the unlinked resistivity Variations.

As noted in previous work, as seawater has resistivity that is orders of magnitude smaller than that of concrete, it is realistic to take the potential distribution at the external submerged portion of the column as space-invariant[5]. For the one-dimensional model used here, all elements for the submerged portion were thus assumed to share a common potential with that block of elements, acting in unison (behaving as if connected to the waterline element by a resistor of value determined by the resistivity assumed for the waterline level and the column dimensions and internodal spacing). Figure 1 shows for completeness the resistivity profile for the rest of the submerged zone, but that part of the profile does not enter in the calculations due to this simplifying assumption.

Oxygen diffusivity was assumed to follow an elevation profile similar to that of concrete resistivity but inversely, to reflect the pronounced decreasing effect of water saturation on oxygen transport in concrete[1]. The extreme values chosen for this parameter is also representative of those reported in the literature.[1] The baseline assumption, in keeping with our previous work[5,20], was to consider an oxygen diffusivity profile that varied exponentially with elevation as illustrated in Figure 1. That assumption was resulted in a region of diffusion-limited oxygen reduction current that extended to relatively large elevations above the waterline. As a variation, an alternative condition where oxygen diffusivity increased linearly with elevation was explored as well.

Following Ref. 20, C_S was assumed to be greatest just above the waterline and decays with increasing elevation (a condition typical in marine installations). C_S was assumed to follow a decreasing linear variation with increasing elevation above high tide. The end values given in Table 1 are representative of regimes encountered in Florida bridges. A nominal value of C_S equal to 3/5 of the waterline/high tide elevation Cs value was assumed for the submerged region, since no evaporative chloride accumulation occurs on the concrete surface. The chosen value of C_{TS} is a commonly assumed conservative value for steel in atmospherically exposed concrete, where the passive steel potential is similar to the choice of E_P used. While the above material properties and boundary conditions are loosely representative of some field conditions, it is emphasized that the values were chosen mainly for illustration of the modeling concept and not to match the behavior of a specific actual system.

Polarization kinetic parameters values for the corrosion reactions are credible and similar to those used in previous modeling approaches[5]. The kinetic parameters representing potentials were chosen to correspond to the copper-copper sulfate (CSE) reference electrode scale. See note in Table 1 for sign conventions.

There is a reasonable agreement on what representative values of E_P and C_{Ts} may be used for those parameters in the relationship between C_T and E, since they would represent the open circuit potential and chloride threshold respectively of unbiased passive steel in concrete, and plausible choices were listed accordingly in Table 1. However, considerable uncertainty exists on the value of β_{CT}, which has been earlier estimated to be in the order of 0.1V/decade [17] but for which recent work suggest as much as 0.4V/decade. Since C_T depends exponentially on the choice of β_{CT}, there is concern about the sensitivity of the model projections to variations in this parameter, which was chosen as a variable for examination. For the baseline case a threshold potential dependence β_{CT} value of 0.4V/decade was assumed, reflecting an extreme suggested by a recent literature compilation[16]. Variations were slopes of 0.2 V/decade and 0.1 V/decade reflecting increasingly optimistic but also more uncertain scenarios. In addition, a potential-independent threshold condition was used as reference, implemented by making $\beta_{CT} = \infty$ so per Equation 8 C_T is fixed at the value C_{TS}.

Another source of uncertainty is that the discretization used in the present model illustration establishes a minimum size of the steel surface that is activated in each initiation event. Moreover, a simplifying assumption was made that the size of the spalled region upon damage declaration was equal to that of the steel element size projected on the external concrete surface. The choice of steel element size, especially in combination with that simplifying assumption, is expected to affect the resulting projected damage function, so element size was also chosen as an investigation variable. Those variations were examined in preliminary work presented elsewhere[20] , with results that will be discussed in the next section.

The activation zone size for one steel element in the baseline case (chosen to maintain consistency with previous work[19]), resulted in a nominal spall size of 0.38 m^2. Variations chosen to investigate sensitivity to this parameter included active zones equal to ½, 2 and 3 times the steel element surface area of the baseline case. The larger cases were simulated by declaring one or two adjacent steel elements respectively to be active upon activation at an individual node. The ½ case was simulated by conducting calculations with twice the number of longitudinal nodes, but keeping the conductance between the waterline node and the submerged portion equal to that used for the other configurations.

The calculations cover the period from 0 to 60 years of age, using a 0.25 years time step, the same values as used previously[20]. Here again, that time step value was found to be fine enough to avoid in most cases multiple activation declarations of adjacent zones in a single time step. In those few instances where two or more adjacent zones were found to have exceeded the value of C_T during a single time step, only the zone with the greatest excess was allowed to become active. The procedure was extended with appropriate allowance to the active zone variation cases. It is noted however that as a result of the assumptions discussed above, submerged portion steel elements were always treated as a single unit and subject to simultaneous activation.

RESULTS AND DISCUSSION

Figure 2 shows the steel potential- and corrosion current density- elevation profiles for the Base case at ages 24y, 27 y, 49y and 60y. The 24 y graph shows also (dashed line) the initial potential profile when the entire assembly was passive. In that condition the anodic reaction occurred uniformly over the entire rebar assembly, at the assumed value of the passive dissolution current density (0.056 $\mu A/cm^2$), which is the background value shown in the current density profile. That current density was below the limiting current density for oxygen reduction so under the simplifying assumptions used the entire assembly existed at the same mixed potential value, which was ~-0.155 V, a value typical of passive steel in concrete. That condition was maintained until the end of year 24, when the waterline steel element was the first to become active. Since the potential was uniform, the value of C_T was also the same throughout. First activation was to be expected at the waterline because C_S was highest there, so chloride buildup at the rebar surface was faster at that element too. Upon activation, the steel there became a net anode and the potential and current density profiles changed into that indicated by the solid line in the 24 y graph. The steel element at that node developed a high corrosion current density, and a distinctly negative potential, as commonly observed upon local steel activation in concrete. The potential depression extended to the nearby, still passive steel elements, reflecting macrocell galvanic coupling. That polarization decreased above water with distance from the active steel element, consistent with macrocell coupling in a resistive electrolyte. At elevations ~>1 m the effect vanished for the most part and the potential approached the initial potential. On the submerged side the steel potential changed abruptly and reached a value somewhat more negative than the initial potential, corresponding to the coupling of the large, still passive (effectively equipotential) submerged zone with the newly activated waterline steel element.

The steel at the newly active spot underwent corrosion at a high rate much as a consequence of this coupling with a locally weak, but overall large cathode. As it will be shown further below, the concrete over the waterline steel element reached damage declaration about 3 years later due to increasing corrosion penetration and consequent accumulation of

corrosion products to the level stated to initiate cracking. Also during the next 3 years chloride concentration built up to higher levels in the surrounding passive steel elements, even exceeding the initial C_T value, but activation did not take place in those elements because the C_T values had increased due to the local potential depression. Instead, the next activation event (year 27, coincidental with damage declaration at the waterline steel element but not related to it) took place at a higher elevation where the preventing effect from the polarization induced by the first anodic zone was lower. That second activation event occurred at a later date than the first because at that higher elevation the surface chloride concentration was lower (and C_T had become a bit higher) than for the waterline steel element. As found previously[20], the second activation created a second negative peak in the potential profile, with associated potential depression and C_T increase in the nearby passive steel elements. The corrosion current density was somewhat smaller than that of the waterline steel element, as macrocell coupling did not include the relatively large underwater cathode.

The next events included additional activations above the waterline as the increasing chloride concentration exceeded the local C_T value, but always some distance away from elements already active (as those delayed corrosion initiation around them). The result was comb-like potential and corrosion current density profiles as seen in the figure for year 49. The corrosion current density was greater at the higher elevation elements because, under the assumed parameter profiles, oxygen diffusivity was greater there so diffusional limitation of the cathodic reaction was less prevalent. Shortly afterwards the entire submerged zone became active, the late date reflecting the lower value of C_S present there and some increase in the value of C_T resulting from the cathodic polarization that had taken place starting with the activation of the waterline steel element in year 24.

The condition with the zone below water activated is shown in the graph for year 60 (end of the simulation). By that time the column potential profile had reached a mature pattern with multiple corroding zones above the waterline, separated by intermediate positions where the cathodic prevention effect delayed activation over a long time frame. The uniform steel activation underwater resulted in potentials that were the most negative in the system, because the cathodic reaction was fully concentration limited in that zone. Consequently the corrosion rates below the waterline were uniformly very low, at a value equal to that of the limiting current density for oxygen reduction (~0.95 $\mu A/cm^2$), about twice that of the passive dissolution current density experienced there before activation. Activation underwater also eliminated the large coupled cathodic region that aggravated corrosion in the waterline steel element. Consequently, the corrosion current density at that element dropped to a value commensurate with the low values prevalent where oxygen transport limitation was important, as noted above.

The potentials and corrosion current densities calculated for the active and passive portions generally approximate those encountered in actual corroding marine structures. Here again, in concert with Ref. 20, for the exploratory purposes of this paper no attempt was made to refine the selection of kinetic parameters to develop a direct comparison to any specific system. It is also important to note that the simultaneous activation for the elements below water is a combined result of the simplifying assumption that all elements there share the same potential, and that C_S and chloride diffusivity are also the same on that entire zone. Those assumptions are clearly unrealistic, but their effect is minimized by the low limiting current density for oxygen reduction in that zone. Preliminary calculations to be published elsewhere treated steel elements below water individually, allowing for activation of one

element ahead of the others. It was seen that as a result the projected rate of corrosion of that one element was large, but also that the effect of the entire mixed submerged zone on the rest of the column was nearly the same as in the simplified case addressed here. Thus, the findings presented here are still relevant to the zone above water, where the manifestations of corrosion are most evident in actual systems. It is also observed that while concentration of corrosion at submerged regions of the rebar assembly could lead to significant local loss of steel cross section, it does not necessarily cause concrete cracking as accumulation of solid corrosion products may be lessened significantly [6 (3)].

Figure 3 (top) shows the cumulative damage function for the Base case (β_{CT}=0.4 V/decade) and variations with smaller values of β (greater dependence on potential) as well as with Fixed C_T (β_{CT}=∞). In the 101 node array used, each single element damage event affects ~1% of the total column surface. By age 60y, ~11% of the surface was affected in the Base case. Since by that age only elements in the above-water half of the column had reached damage declaration, the above water damage was ~22%.In all the projections the damage function has an uneven, stepwise quality reflecting successive activation and propagation events at different elevations, and the relative corrosion-preventing influence of each newly activated element according to its local corrosion rate and the effective resistance of the concrete path to nearby elements. Some minor contribution of the finite time step used (0.25 years) existed as well but it was secondary in nature. It is emphasized that while the damage projection may appear to consist of random steps, the projection is entirely deterministic and not the result of a probabilistic assignment of corrosion initiation events or propagation rates, as it is used in other forecasting approaches [9,10]. It is also noted as an independent validity check that the simplified one-dimensional model generally approximated the results of a 2-dimensional rotational symmetry model with similar base parameters used in our previous work[19].

When there is no threshold potential dependence and all other parameters are as in the Base case, the first activation event still occurred at the waterline steel element. That event occurred at nearly the same time as in the Base case (the small difference was due to the open circuit potential of the all-passive assembly being some 30 mV lower than the chosen E_P value). Unlike in the Base case, activation of the nearby elements at increasingly higher elevations occurred very soon after the first event, since no protection of surrounding steel elements was derived from the first or subsequent active zones (as found previously[20]). Thus a continuum of active steel tended to form as the chloride front progresses activating an ever widening portion of the rebar assembly. The more uniform distribution of corrosion resulted in less macrocell action compared with the Base case. Oxygen demand affected a larger region and as a result the local corrosion rates tend more to be limited by oxygen supply, which was less at the lower elevations following the assumed oxygen diffusivity profile. In those regions the time interval between activation and damage declaration was much greater than in the Base case, and for many of those elements concrete damage was not reached by year 60. An exception was the waterline element, which because of the low resistivity path to the submerged region had efficient galvanic coupling with the still passive large region below waterline. Thus the waterline element reached concrete damage declaration after only about 3 years following steel activation. At increasingly higher elevations the oxygen diffusivity was

[3] This is not to dismiss the possible structural effects of steel corrosion below the waterline, which have received much less attention in the literature, in part because of sparse field investigation evidence. The modeling approach presented has significant potential to better understand that issue.

higher, local corrosion rate was higher, and the local damage declaration was reached increasingly sooner after activation. Although the damage condition for the first elements activated above the waterline was reached later than in the Base case, there were many more active steel elements than in the Base case. Thus for the fixed threshold case (with all else as in the Base case) the damage function rose comparatively much faster even though it started accelerating somewhat later than in the cases with potential dependent threshold. That delay in acceleration essentially disappeared for the faster oxygen diffusivity variation (D_{O2} increasing linearly with elevation) results shown in Figure 3 (bottom) since the oxygen supply there was fast enough to allow for significant corrosion rates closer to the waterline with less dependence on macrocell coupling. For the same reason the projected terminal damage levels for the fixed C_T and lower potential dependence cases were also higher when oxygen was allowed to become more available at the lower elevations.

The damage function in the fixed-threshold cases had too a stepwise appearance, although not as pronounced as in the potential-dependent cases. Again, the steps do not reflect random events but instead result mainly from the deterministic combination of a finite node array, a growing uneven chloride penetration front, and variations in the propagation times of different steel elements.

The damage projection for the potential dependent threshold cases was, as expected from the form of Eq. 8, slower as β_{CT} was smaller. However, even though C_T depends exponentially on β_{CT}, for the conditions examined the variation of projected damage after 60y service differed by only roughly a factor of two or three when varying β_{CT} from 0.4 V/decade to 0.1 V/decade, a range noted above to reflect available data and proposed working values. The sensitivity to the choice of that slope, within a range of plausible values, was moderate considering the uncertainty in other parameters that may affect the model projection. The sensitivity to potential dependence is further illustrated in Figure 4, where the damage projected for 60y age ($Damage_{60y}$) is plotted as function of $1/\beta_{CT}$ for which zero in the abscissa corresponds to the Fixed C_T case. The graphs show that trends seen in Figure 3 were generally maintained over all the concrete resistivity (see further discussion below) and oxygen diffusivity variation cases. After the significant change from no threshold potential dependence to β_{CT} = 0.4 V/decade ($1/\beta_{CT}$=2.5) the value of $Damage_{60y}$ decreases relatively slowly in all cases with a slope $d \log(Damage_{60y})/ d \beta_{CT}^{-1} \sim 0.5$ V.

The dependence of projected damage on concrete resistivity is summarized in Figures 5(a) (resistivity only varied) and 5(b) (linked resistivity - D_{Cl-} variations[27]) again using $Damage_{60y}$ as the metric. In both scenarios the projected damage was, as expected, the highest for the Fixed C_T cases. Because much of the projected damage in those cases occurred relatively early, the 60y results tended not to be strongly differentiated, except for showing clearly greater damage when oxygen access was faster. When only the resistivity was varied $Damage_{60y}$ increased only slightly as resistivity decreased. Linking lower resistivity with faster chloride diffusion resulted in a more appreciable increase in $Damage_{60y}$ as resistivity decreased. Those trends are in keeping with expected behavior under fixed C_T.

The potential dependent threshold cases showed markedly different responses to the effect of lowering resistivity, depending on whether linking with D_{Cl-} changes was assumed or not. When only resistivity changed, the projected amount of damage consistently decreased with decreasing resistivity. This behavior may seem surprising, as the usual expectation is that more damage would result from decreasing concrete resistivity. However, as D_{Cl-} was kept

constant, the main effect of the change was to create more efficient macrocell coupling. Better coupling allowed the corrosion prevention effect to act on a large portion of the column, thus delaying the spread of the onset of corrosion. The model results indicate that the delay (and consequently less number of active steel elements) had a greater impact on reducing the overall damage accumulation than any intensification of local damage at the elements that may have resulted from the more efficient coupling with nearby cathodes once activation took place. Remarkably, the relative effect was approximately the same in all β_{CT} variations considered and for both oxygen availability variations.

The calculations with the more realistic assumption of linked resistivity and D_{Cl^-} variations yielded projections that, for the high resistivity end of the range investigated, did meet usual expectations. However, for increasing lower resistivity values the projected damage began a downward trend that, although less marked than in Figure 5(a), was still important. Thus, even in this scenario the threshold elevation due to the increase in macrocell coupling, once it become strong enough, still had a dominant beneficial effect. The present simulations involve sweeping simplifications, including the assumption of an elevation-independent value of D_{Cl^-}. Nevertheless, these results underscore the dramatic effect that inclusion of threshold potential dependence can have on projected damage and its dependence of system parameters.

Results from variations where each activation event affects ½, 2 or 3 times the surface of the steel associated with one node, investigated earlier [20] are shown in Figure 6 again using the value of $Damage_{60y}$ as a descriptor. Resistivity, oxygen diffusivity and β_{CT} were kept constant as for the Base case. The damage projection was clearly sensitive (roughly proportional) to the choice of the activation zone size. The result is partly due to the choice of model formulation and parameters used in these illustrations. In particular, the one-dimensional treatment leading to Eq.(7) does not include provision for local resistance polarization. Consequently, the use of a simply activation-polarized formulation for the anodic reaction with a relatively small Tafel slope results in net anodic currents for active steel elements that vary little with element size in the range investigated. Accordingly, the prevention effect on surrounding steel is comparable and calculations tend to project about the same number of active elements at a given time in all cases investigated. While those conditions do affect the length of the individual propagation stages, the overall behavior in the present illustration tends to be initiation-stage dominated so the progression of number of projected spalls was not changed substantially. Furthermore, as the spalls are assumed to be equal in size to the projection of the active zone on the external concrete surface, it is not surprising that the extent of damage progression was approximately proportional to the choice of active zone size.

The above observations point to opportunities for refinements in subsequent model realizations, in what pertains to sensitivity to activation zone size in the one-dimensional model. Those refinements should include attention to a formulation that recognizes local resistance polarization especially when activation zone sizes are small, realistic anodic polarization functions, and incorporation of more detailed relationships between spall and active zone size[6]. Alternatively, experimental observations may provide evidence of activation zone sizes and related spall sizes to be used as a direct model input for specific classes of systems to be modeled. In the context of the overall model formulation, the use of only a simplified one dimensional model does not permit interaction between active and passive zones at different perimeter positions at a given elevation. That limitation impacts not only the

issue of activation zone size, but also much of the items discussed earlier. Incorporation of multidimensional treatments, as explored elsewhere [19,22] will be necessary depending on the extent to which detailed solutions are needed.

Building upon preliminary findings [19,20], the present work served to illustrate the concept of integrating threshold potential in a novel combined initiation-propagation predictive model, by means of exploratory applications. Important insight on key durability factors was readily obtained. In particular, the calculations showed that ignoring potential dependence of the threshold could lead to overestimating damage projections. The calculations served also to highlight limitations in the model that need addressing toward eventual application of the concept in practical forecasting procedures. Continuation work is in progress to address those issues.

CONCLUSIONS

Functionality was demonstrated for a deterministic model that projected corrosion damage in a partially submerged reinforced concrete column, incorporating potential dependence of the chloride threshold and macrocell coupling of regions that were at different local stages of corrosion initiation and propagation.

Introduction of threshold dependence of potential resulted in lower damage projections compared with a fixed threshold case. The effect was stronger, as expected, when the slope of the assumed log of threshold concentration vs. potential relationship was smaller. The sensitivity to the choice of that slope, within a range of plausible values, was moderate considering the uncertainty in other parameters that may affect the model projection.

The decrease in projected damage progression from introducing threshold dependence on potential tended to be more marked when the concrete resistivity was smaller, reflecting more efficient macrocell coupling along the column. That effect remained over much of the range investigated even after linking the decrease in resistivity with an increase in chloride diffusivity. Oxygen availability tended to play a secondary role on the extent of the effect of introducing threshold dependence on potential.

The damage projection for cases with potential dependent threshold decreased as the activation zone size became smaller. Model development approaches to resolve that limitation were identified.

ACKNOWLEDGEMENT

This investigation was partially supported by the Florida Department of Transportation. The opinions and findings stated here are those of the authors and not necessarily those of the funding agency.

REFERENCES

1. K. Tuutti, Corrosion of Steel in Concrete (ISSN 0346-6906) Stockholm, Sweden: Swedish Cement and Concrete Research Institute, 1982.

2. M.D.A. Thomas, E.C. Bentz, “Life365-Computer Program for Predicting the Service Life and Life-Cycle Costs of Reinforced Concrete Exposed to Chlorides,” ver.1.0.0 (Potomac, MD:The Concrete Corrosion Inhibitors Association, 2000).

3. E. Samson, J. Marchand and J. Beaudoin, Cement and Concrete Research V. 30 (2000) p.1895.

4. R.E. Weyers, B.D. Prowell, I.L. Al-Qadi, M.M. Sprinkel, M. Vorster, “Concrete Bridge Protection, Repair, and Rehabilitation Relative to Reinforcement Corrosion: A Methods Application Manual,” SHRP-S-360 (Washington, DC: National Research Council, 1993.)

5. S.C. Kranc and A.A. Sagüés, Corrosion, Vol. 50, p.50, 1994.

6. A. Torres-Acosta and A. Sagüés, ACI Materials Journal, Vol. 101, p.501, 2004.

7. P.D. Cady, R.E. Weyers, J. Trasp. Engrg. 110, 1(1984) p.35-44

8. A. Ramniceanu, R., Weyers, J., Riffle, M. and Sprinkel, ACI Mat. J. V. 105, p. 459, 2008

9. E. Bentz, ACI Materials Journal, Vol. 100, p.391, 2003.

10. A.A. Sagüés, Corrosion, Vol. 59, p.854, 2003.

11. G. Williamson, R. Weyers, M. Brown, A. Ramniceanu, and M. Sprinkel. ACI Materials Journal, Vol. 105, p.375. 2008.

12 L. Li, A.A. Sagüés, Corrosion, Vol. 58 p.305, 2002

13. L. Li, A.A. Sagüés, Corrosion, Vol. 57 p.19, 2001

14. K. Lau, A.A. Sagüés, L. Yao, and R.G. Powers. Corrosion, Vol. 63. p.366, 2007

15. C. Alonso, M. Castellote, C. Andrade, Electrochim. Acta Vol. 47, p. 3469, 2002.

16 F.J. Presuel-Moreno, A.A. Sagüés and S.C. Kranc, Corrosion Vol 61, p428, 2005.

17. L. Bertolini, F. Bolzoni, T. Pastore and P. Pedeferri, "New Experiences on Cathodic Prevention of Reinforced Concrete Structures", pp. 390-398 in Corrosion of Reinforcement in Concrete Construction", C. Page, P. Bamforth and J. Figg, Eds., Society for Chemical Industry, Special Publication No. 183, London, 1996.

18. J. Broomfield. Corrosion of Steel in Concrete: Understanding, Investigation and Repair. London: E&FN Spon, 1997.

19. A.A. Sagüés and S.C. Kranc, Model for a Quantitative Corrosion Damage Function for Reinforced Concrete Marine Substructure” , in Rehabilitation of Corrosion Damaged Infrastructure, p.268, Proc., Symp. 3, 3rd. NACE Latin-American Region Corrosion Congress,

P.Castro, O.Troconis and C. Andrade, Eds., ISBN 970-92095-0-7, NACE International, Houston, 1998.

20. A.A. Sagüés, S.C. Kranc, and K. Lau. “Modeling of Corrosion of Steel in Concrete with Potential-Dependent Chloride Threshold” to be published in the Proceedings from the 17th International Corrosion Congress, Las Vegas, NV, October 6-10, 2008. Paper No. 4006. NACE International, Houston, TX.

21. Z. Szklarska-Smialowska, Pitting Corrosion of Metals. NACE, Houston. 1986.

22. S.C. Kranc and A.A. Sagüés, "Development of Damage Functions to Predict the Durability of Steel Reinforced Concrete Structural Elements", presentation at Corrosion-Conference on Understanding Corrosion Mechanisms in Concrete, M.I.T., Cambridge, Mass., 27-31 July, 1997.

23. L. Bertolini, B. Elsener, P. Pedeferri, R. Polder. Corrosion of Steel in Concrete: Prevention, Diagnosis, Repair. Germany: Wiley-VCH, 2004.

24. C. Andrade, C. Alonso, J. Rodriguez and M. Garcia, "Cover Cracking and Amount of Rebar Corrosion: Importance of the Current Applied Accelerated Tests", pp. 263-273 in Concrete Repair, Rehabilitation and Protection, R. Dihr and M. Jones, Eds, E&FN Spon, London, 1996.

25. F. J. Presuel-Moreno, S.C. Kranc, A.A. Sagüés, Corrosion, Vol. 61, p.548, 2005

26. H. Kaesche, Metallic Corrosion. NACE, Houston. 1996.

27. A.A. Sagüés et al, “Corrosion Forecasting for 75-Year Durability Design of Reinforced Concrete,” Final Report to Florida D.O.T. WPI 0510805. Dec. 2001, Available online, www.dot.state.fl.us.

28. C. Andrade, O. Rio, A. Castillo, M. Castellote, and R. d’Andrea. ECCOMAS Thematic Conference on Computational Methods in Tunnelling. MSO4-2, 68. Vienna, Austria. August 27-29, 2007.

29. A. Bentur, S. Diamond, and N.S. Berke. Steel Corrosion in Concrete: Fundamentals and Civil Engineering Practice. London: E&FN Spon, 1997.

30. A.A. Sagüés et al. “Corrosion Forecasting for 75-Year Durability Design of Reinforced Concrete.” Final Report to Florida D.O.T. WPI 0510805. Dec. 2001. Available online, www.dot.state.fl.us

TABLE 1

MODEL PARAMETERS*

(Refer to Figure 1 for key)

Steel Cover	Xc =	10.5 cm
Column diameter	Φ=	105 cm
Column Length	L=	1200 cm
Concrete Resistivity	ρ_H=	$2\ 10^5$ ohm-cm (Base); x1/3, 1/10 (Variations)
	ρ_L=	$4\ 10^4$ ohm-cm (Base); x1/3, 1/10 (Variations)
Oxygen Diffusivity	D_{OH}=	10^{-3} cm^2/sec
	D_{OL}=	10^{-5} cm^2/sec
		Log D varies linearly with elevation (Base)
		D varies linearly with elevation (Variation)
Chloride Diffusivity	D_{Cl}-=	$2\ 10^{-8}$ cm^2/sec (Base); x ρ_{LBase} / $\rho_{LVariation}$ (Linked Variations)
O_2 Surface Concentration	C_{SO}=	$2.5\ 10^{-7}$ mol/cm^3 (in pore water)
Cl^- Surface Concentration	C_{SH}=	15 Kg/m^3
	C_{SW}=	9 Kg/m^3
	C_{SL}=	0 Kg/m^3
Chloride Threshold Parameters	C_{TS}=	0.71 Kg/m^3
	E_p=	-128 mV
	β_{CT} =	400 mV/decade (Base);
		200 mV/decade, 100 mV/decade, Fixed C_T (Variations)

Polarization Parameters**	E_0 (-mV CSE)	i_0 (A/cm^2)	Tafel Slope (mV)
Iron Dissolution	-780	$1.875\ 10^{-8}$	60
Oxygen Reduction	+160	$6.25\ 10^{-10}$	160

Steel Passive Current Density	$i_p = 0.058\ 10^{-6}$ A/cm^2
Critical Corrosion Penetration	P_{CRIT} = 0.01 cm
Active Zone Size	Corresponding to 1 node (Base)
	Corresponding to ½ base case node, 2 nodes, 3 nodes (Variations)

* To provide a rough check on model operation, system parameters and configuration were chosen to be comparable to those used in earlier 2-dimensional cylindrical geometry calculations presented in Ref. 5. Concrete resistivity was assigned twice the earlier value to compensate somewhat for differences in the effective conductive path resulting from the assumptions used here.

**Potentials are presented in this table and the results using the usual electrochemical convention where the rate of anodic reactions increases as the potential becomes more positive. Equations in the text however address potentials in the electrolyte with effectively the opposite convention.

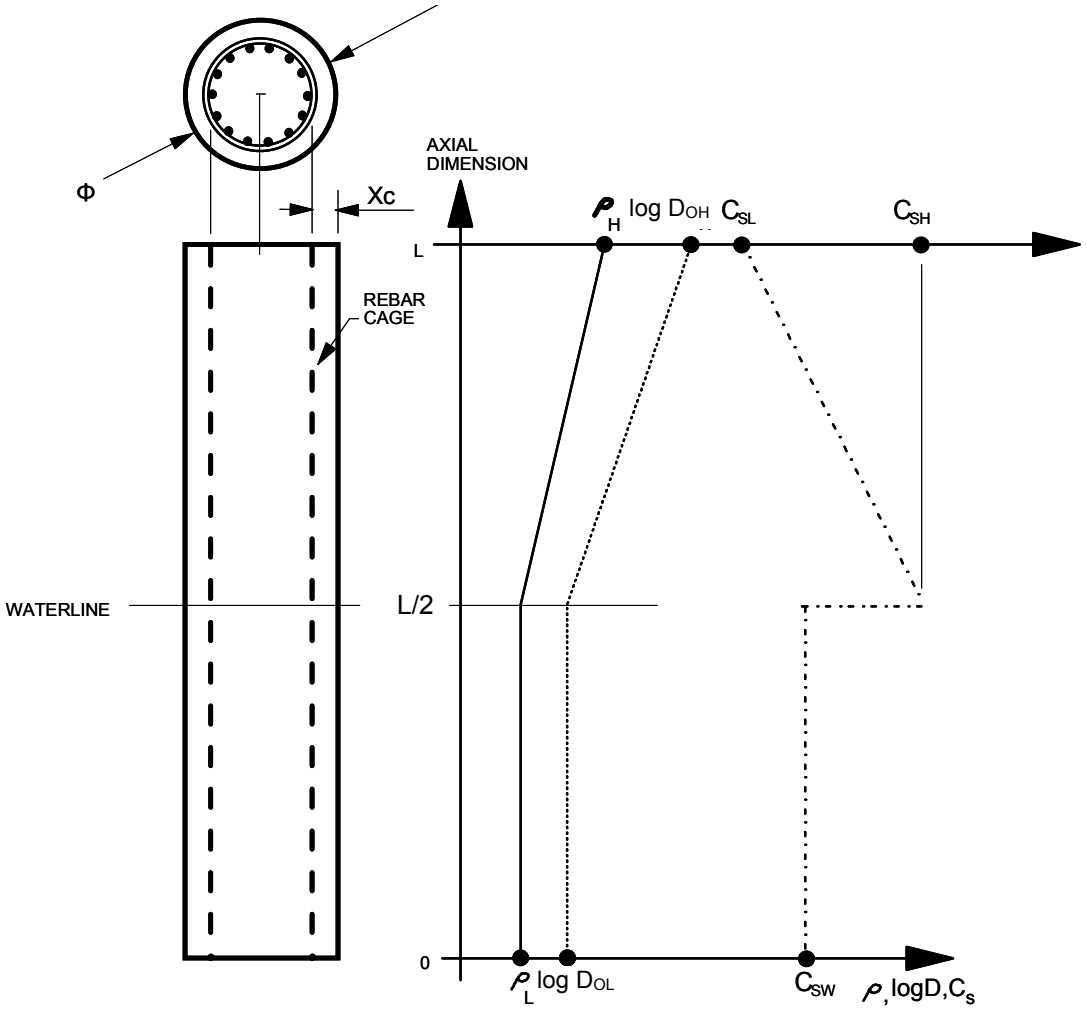

FIGURE 1 - System modeled[19], Base scheme.

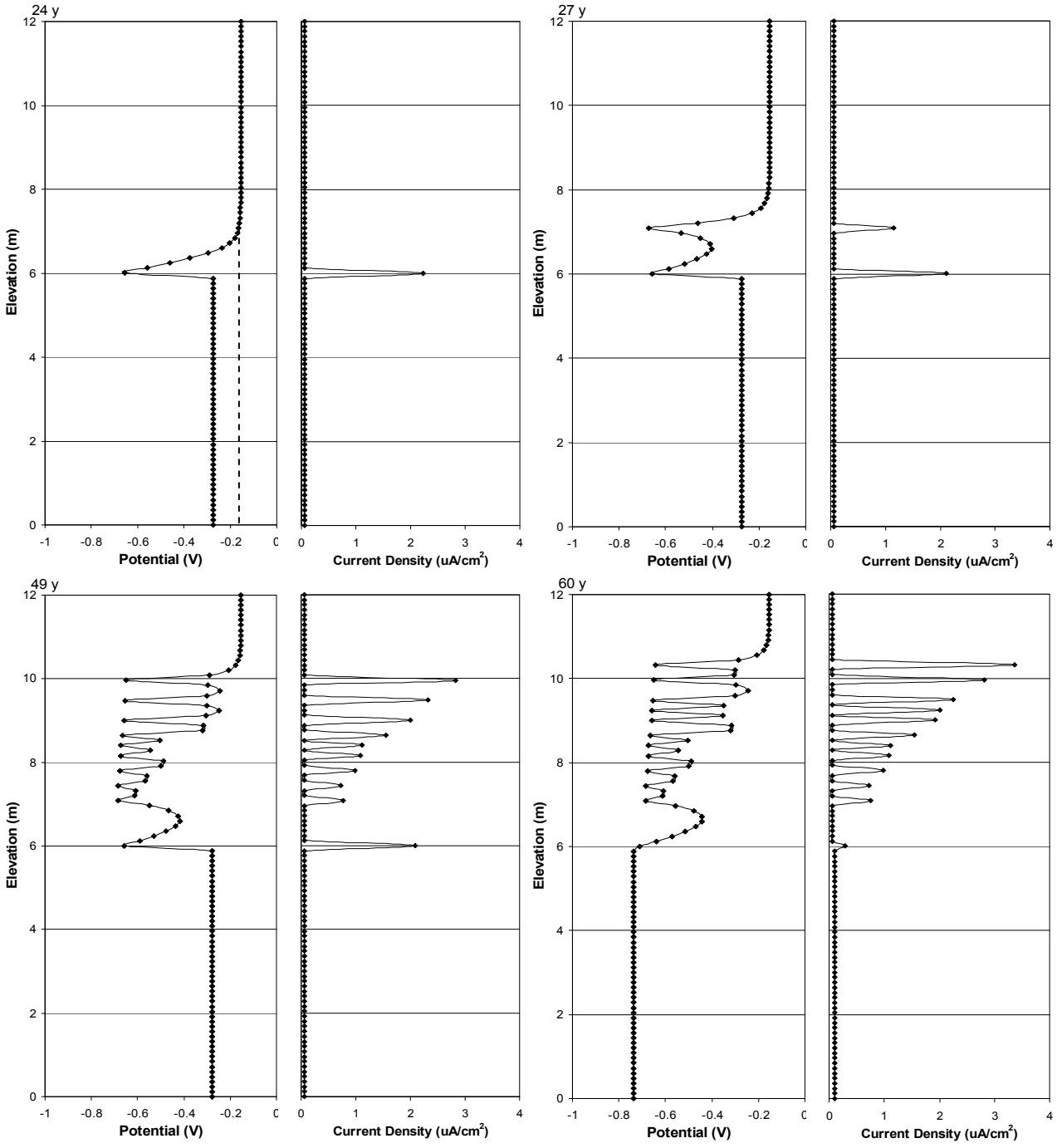

Figure 2 – Evolution of potential- and corrosion current density-elevation profile as function of age, Base Case. The dashed line is the initial potential profile of the all-passive assembly. 24 y: first activation event. 27 y: second event. 49 y: just before activation of submerged portion. 60 y: mature pattern.

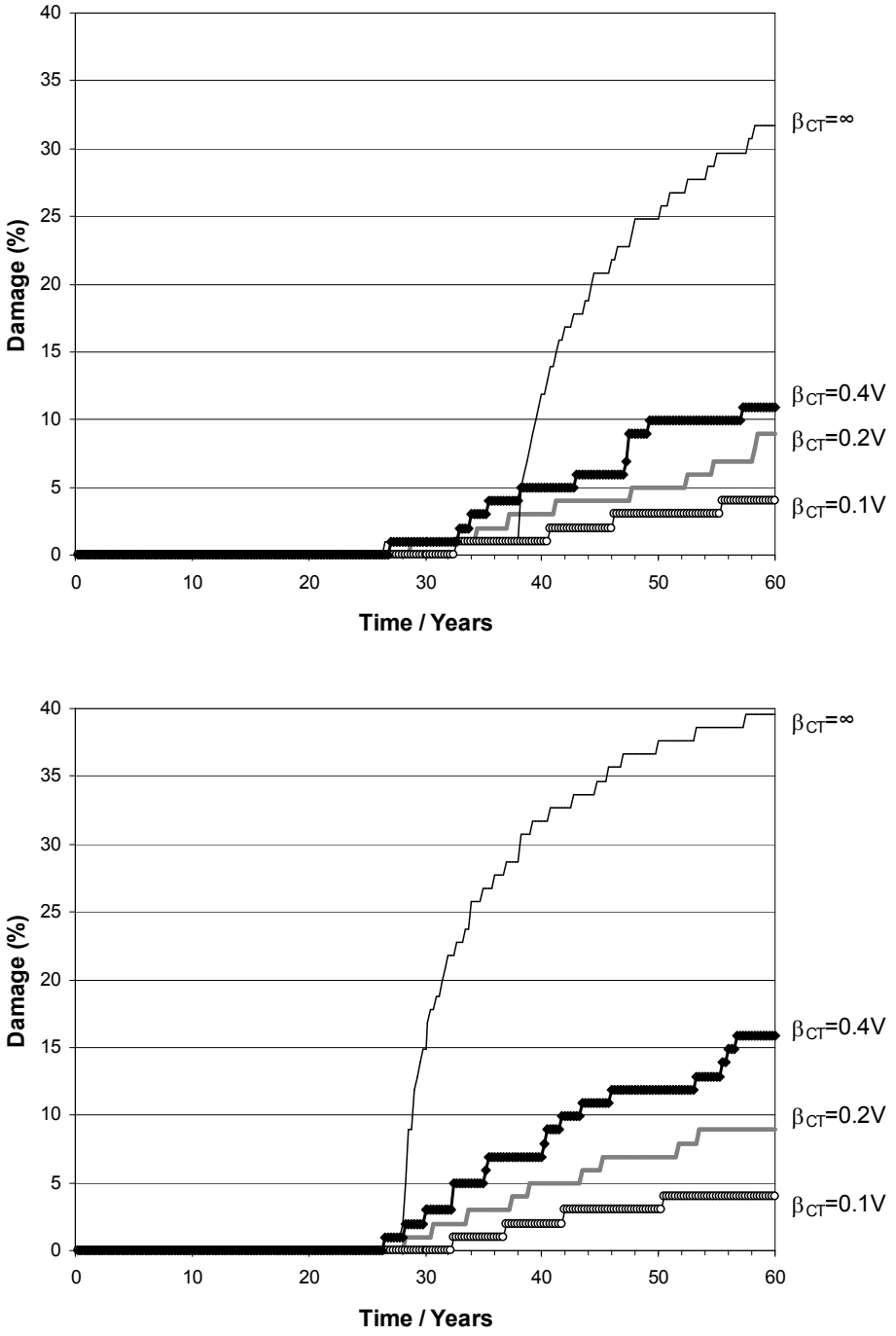

Figure 3 - Top: Damage projections for all parameters as in the Base case except for C_T slope variations . Bottom: Same except for variation with faster oxygen transport.

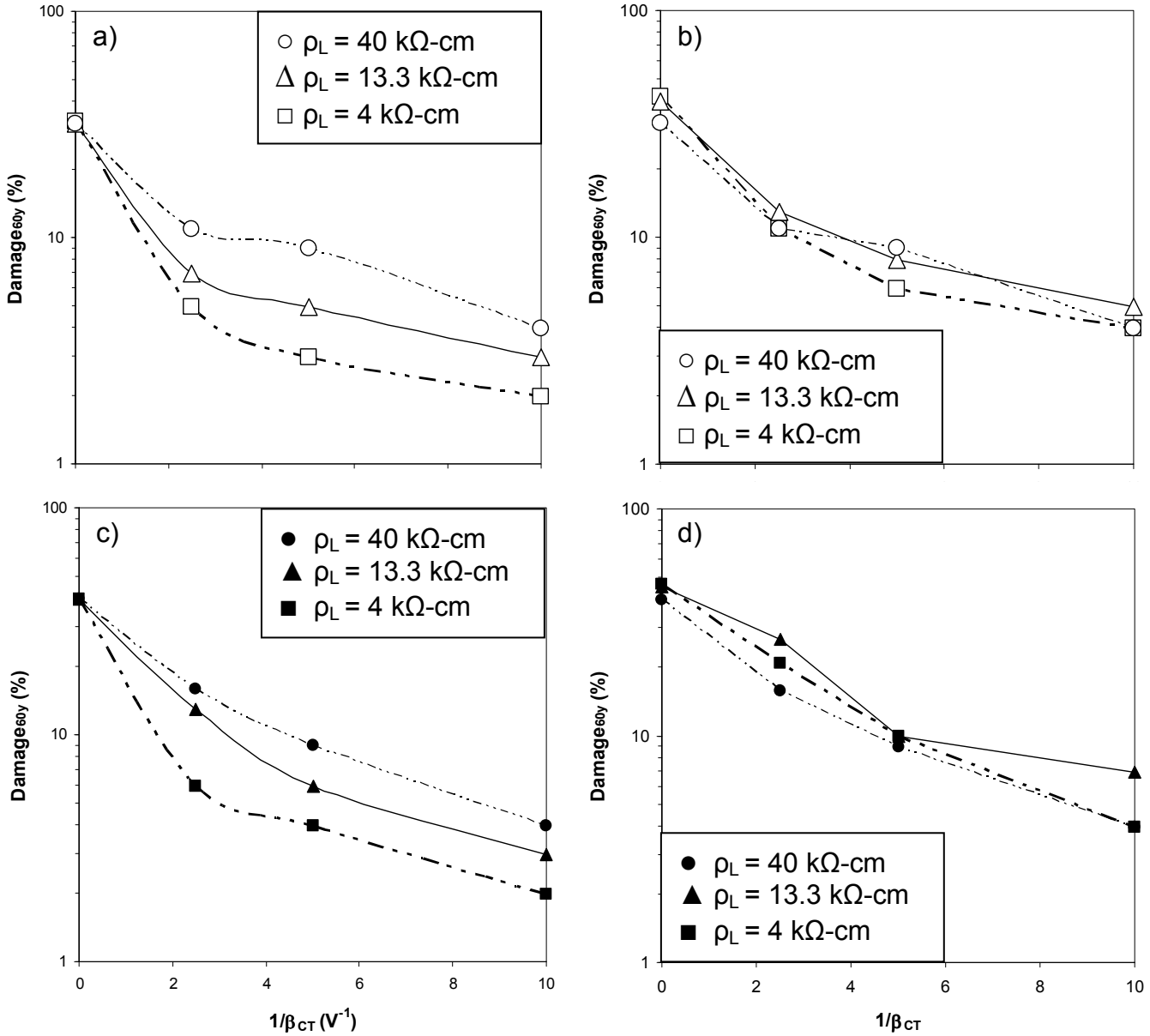

Figure 4- Damage projection for age= 60y. Effect of oxygen transport and concrete resistivity variations. (a) Base case with resistivity not linked to D_{Cl^-} ; (b) Linked; (c, d) Same as (a,b) except for variation with faster oxygen transport.

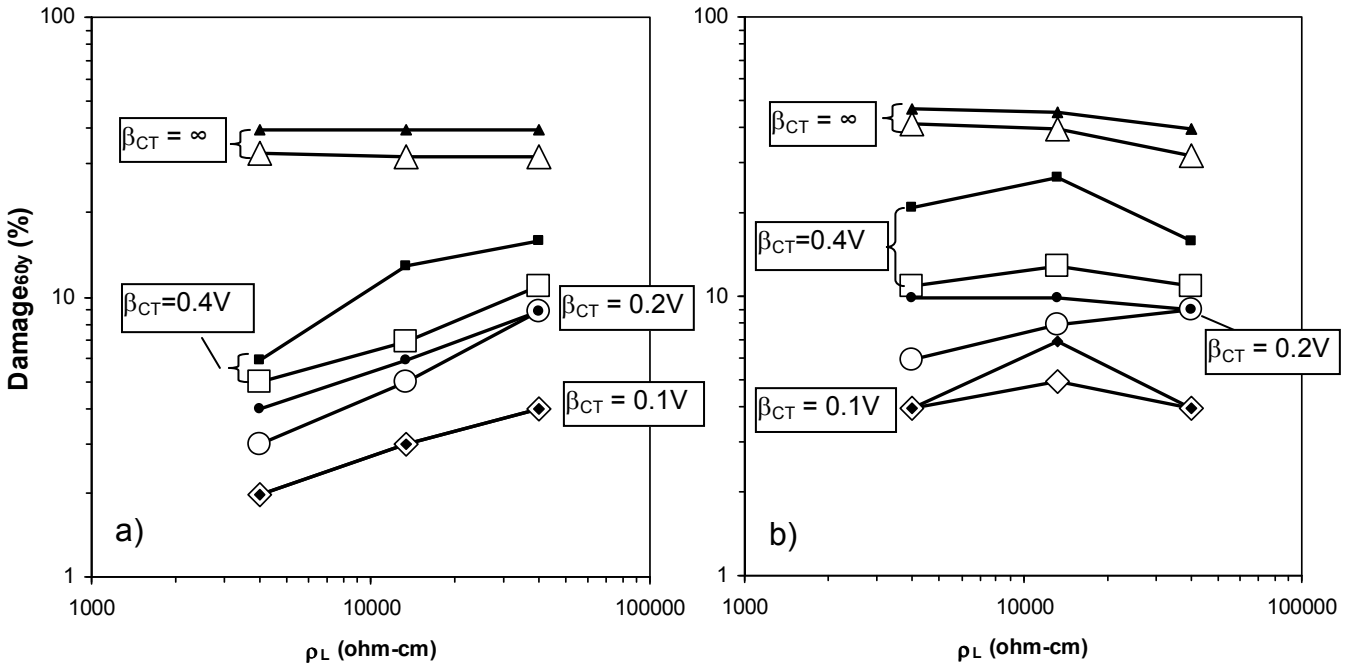

Figure 5 - Combined effect on damage projection for age=60y of variations of concrete resistivity, threshold dependence slope, and oxygen transport (slower: open symbols, faster: filled symbols). (a): D_{Cl-} held at Base case value. (b): D_{Cl-} changes inversely to resistivity variation.

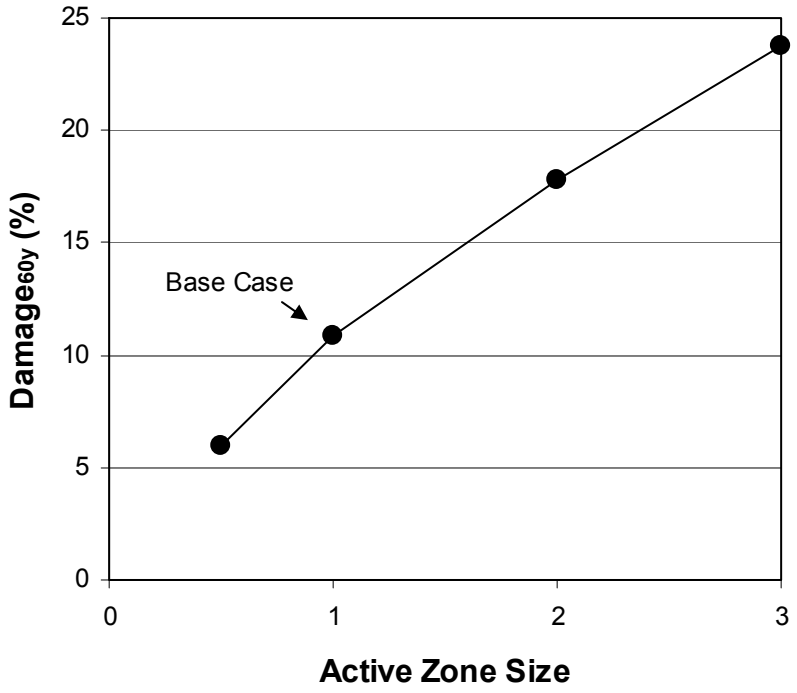

Figure 6. Damage projection for age=60y for varying active zone size (amount indicated is relative to Base case)[20].